



Behavior of a Foundation Built on Geogrid-Reinforced Sand in the Presence of Twin Subsurface Voids

Michael Kazemzadeh¹ · Pantea Pezeshkian¹ · Amirali Zad¹ · Maryam Yazdi¹

Received: 17 May 2024 / Accepted: 24 August 2024
© The Author(s), under exclusive licence to Springer Nature Switzerland AG 2024

Abstract

Underground voids can affect the stability of a foundation and increase structural settlement, especially when they are located directly beneath the foundation. They can arise from a range of sources, including natural formations and buried infrastructure. If these voids interact with the foundation, they can lower its bearing capacity, making them hazardous and costly to remedy. The behavior of soil having a single void has been the subject of past research, but few studies have examined the behavior of soil with twin voids. The current study used physical modeling to examine the effect of the use of geogrids on the behavior of a sandy bed with twin voids. The variables examined included soil density, void embedment ratio, void distance ratio and the number and vertical spacing of the geogrid layers. The use of scaled reinforcements sets this study apart from comparable investigations. Particle image velocimetry was used to examine the development of the failure wedge and the strain rate produced at the surface. The outcomes indicated that both an increase in soil density and the number of geogrid layers greatly increased the soil load-bearing capacity. The bearing capacity of dense soil reinforced with two layers of geogrid increased by 51.8% compared to dense soil without reinforcement. The shear strain rate at the critical slip surfaces beneath a foundation built on dense soil decreased strongly with the use of two geogrid layers.

Keywords Geogrid · Bearing capacity · Twin voids · Reinforced soil · Soil compaction

Introduction

The foundation of a building is the lowest part of a structure and plays an important role in its strength and stability. The soil type, foundation depth, building weight, weather conditions and underground voids all can have an effect on foundation settlement. The existence of underground voids in the areas affected by the incoming forces can reduce the bearing capacity of the soil and increase soil settlement. Such voids can be natural or caused by human activity.

Underground voids can cause the soil to settle under a structure, which can result in damage as well as financial and human loss. One way to prevent such settlement and increase the bearing capacity of the soil is to reinforce the soil [1–16]. The use of geosynthetic reinforcement has increased with the increase in construction in hazardous locations brought about by population growth. The use of geosynthetically reinforced soil (GRS) has become a popular, economical and environmentally friendly technique. However, predicting the bearing capacity of GRS structures located over voids can be difficult, especially for construction projects in void-prone locations.

Past research has investigated the consequences of the use of geosynthetic reinforcements to soil containing a void. Baus and Wang [17] investigated the bearing capacity of foundations located over a void in silty clay using experimental and numerical finite element modeling. Their results showed that there is a critical depth for each foundation below which the void will have a negligible effect on the performance of the foundation. They also showed that the bearing capacity of a foundation over a void above the critical depth will vary according to factors such as the size

✉ Amirali Zad
a.zad@iauctb.ac.ir
Michael Kazemzadeh
michaelkazemzadeh1@gmail.com
Pantea Pezeshkian
panteapezeshkian@gmail.com
Maryam Yazdi
yazdi_ma@yahoo.com

¹ Department of Civil Engineering, Central Tehran Branch, Islamic Azad University, Tehran, Iran

and location of the void and the embedment depth of the foundation. Wang and Badie [18] evaluated the effect of an underground void on the stability of a shallow foundation located on clayey soil. The results showed that the critical depth depends on factors such as the shape of the foundation and of the void, the direction and size of the void and the soil type.

Dash et al. [19] evaluated the behavior of a strip footing placed on a sandy bed reinforced by a geocell mattress. Dilation-induced load transfer from soil to geocell suggests that filling the geocells with denser soils can improve footing performance more effectively. Dash et al. [20] investigated how several types of reinforcement such as geocell, planar, and randomly distributed mesh elements behaved in sand beds when subjected to strip loading. The findings show that, among the soil reinforcement techniques examined, geocell reinforcement provides the most benefits. Latha and Murthy [21] used triaxial compression experiments to examine how the form of reinforcement affected the strength increase of geosynthetic-reinforced sand. The cellular kind of reinforcement is shown to be more effective than the other forms of reinforcement in terms of increasing strength.

Sireesh et al. [22] investigated the bearing capacity of a circular foundation placed on clayey soil reinforced with geocells. The results indicated a significant improvement in the performance of soil reinforced with geocells of sufficient size. Moghaddas Tafreshi et al. [23] conducted an experimental study to evaluate the behavior of a strip foundation on a sandy bed reinforced with geogrids above a void. The results demonstrated that the bearing pressure and settlement of the foundation increased with an increase in the sand relative density, the void placement depth and the number of reinforcing layers caused by arching of the soil mass over the void.

Kiyosumi et al. [24] used 1 g loading experiments to examine the behavior of shallow foundations placed on stiff ground with continuous square voids. According to the findings, the lower void had almost no effect on the failure mode and, as a result, very little effect on the lowering of bearing capacity if two voids in a serial configuration were located at a relatively shallow depth. Sitharam and Hegde [25] developed an analytical model to predict the load-bearing capacity of soft clayey soil reinforced by geocell and a combination of geocell and geogrid. The combination of the geocell and the geogrid is always more advantageous than utilizing the geocell alone, according to the experimental and analytical study results.

Asakereh et al. [26] investigated the behavior of a foundation placed on unreinforced and geogrid-reinforced sand containing a void under the effect of static and cyclic loading. The results showed that the foundation on sand with a

thick geogrid performed better under cyclic loading than the foundation on unreinforced sand without a void. Huckert et al. [27] conducted laboratory tests to evaluate the behavior of an embankment placed on top of a void. In their research, the voids were simulated under granular embankments and the soil layers were reinforced with geotextiles. The results showed that the rupture mechanisms were different for granular soil and reinforced soil layers.

Feng et al. [28] used an analytical method to predict the load acting on geosynthetics located in soil over voids. Their results indicated that the use of non-linear failure criteria can better describe the stress and deformation of the soil and geosynthetics and that ignoring the non-linear behavior of the soil reduced the pressure of the soil on the geosynthetics. Lai et al. [29] studied the types and behavior of rupture in low-height embankments reinforced with geogrids above voids in Plaxis 2D software. They found that the ultimate bearing capacity reduction factor increased as the embankment height increased.

Zhou et al. [30] used the discontinuity layout optimization approach to study the bearing capacity and failure mechanism of a foundation laid on the soil above a void. The results revealed a direct relationship between the failure mechanism and specific soil parameters, as well as the horizontal distance between two voids and the locations of single voids. Wu et al. [31] used the finite element limit analysis approach to assess the effects of void shape, embedment depth, and spacing, as well as variations in soil shear strength, on the bearing capacity of foundations constructed on soil with single and double voids. According to the analysis of the study's findings, the bearing capacity's sensitivity to load eccentricity rose as the distance between the two voids increased.

Geosynthetic-reinforced soil arching was investigated by da Silva Burke and Elshafie [32] using a series of centrifuge experiments. Using soil stress measurements and soil and geosynthetic deformation observations, they inferred the arching behavior. According to the results, arching, rather than forming a physical arch as some models predict, greatly reduces stress at the soil base when a void arises. This is because tension is redistributed. da Silva Burke and Elshafie [33] carried out centrifuge tests to evaluate the deformation of geosynthetic-reinforced soil in response to the development of an underlying void. It was evident from the centrifuge tests that the geosynthetic material next to the void was being stretched and displaced. Anaswara and Shivashankar [34] conducted a numerical study to investigate the behavior of two adjacent strip foundations on clayey soil with voids. The effects of the thickness of the granular bed, length of reinforcement, number of reinforcing layers and presence of voids under the foundation in weak soil on the behavior of foundations were investigated. The results indicated that

the bearing capacity increased with an increase in the thickness of the granular bed up to the optimal thickness and then remained constant for foundations on a granular bed.

Using the finite difference approach, Chaabani et al. [35] examined the effect of placing geotextiles at the interface between a clayey and sandy soil layer on the performance of a foundation built on the aforementioned layered soil with a void. The study's findings demonstrated that when a void is present in the foundation's failure zone, it has a negative impact on the behavior of the foundation. Tizpa et al. [36] used a combination of the finite difference and the discrete element approach to assess the influence of a subsurface void on the response of a shallow circular foundation placed on a granular embankment over cohesive soils. The study's findings demonstrated that the void's negative effect on bearing capacity diminishes as the void's horizontal distance from the foundation's central axis increases, as does the ultimate bearing capacity ratio.

To assess the influence of spherical voids—both eccentric and centric—on the failure mechanisms and bearing capacities of square and circular footings, Khosravi et al. [37] carried out a three-dimensional parametric analysis. The study's findings indicated that an increase in the void's eccentricity ratio and surcharge coefficient leads the Footing's bearing capacity to decrease and increase, respectively. Naftchali and Bathurst [38] employed Flac2D software to develop a hyperbolic isochronous load-strain model in order to study the effect of polymeric geosynthetic reinforcements' rate-dependent properties on the tensile strains of the reinforcements as well as the vertical load and deformation at the reinforcement level and the embankment's surface above a void. The outcomes of the research demonstrated that the maximum tensile strains and loads of the reinforcement are produced precisely above the void's center if the reinforcement's maximum strain does not exceed 5%.

While this field has received little attention in previous research, this work offers an innovative look at how footings that are placed over twin voids in sandy soil behave. This

work stands out for its innovative application of reduced-scale geosynthetic materials for reinforcement and its comprehensive investigation of the bearing capacity-related impacts of soil density, void spacing, and the number of geogrid layers. An even more detailed understanding of the failure mechanisms at work is provided by the use of particle image velocimetry (PIV) to visualize failure wedges. The stability of foundations over diverse and void-prone soils is crucial in civil engineering, where this research directly affects practice. To reduce the danger of differential settlement and structural collapse, the findings can be used to inform the design and construction of buildings, bridges, and other infrastructure on sites with underlying voids. The research findings can be utilized to create sophisticated ground reinforcement plans, like the best location for geogrids and improved methods for compacting soil, that are customized to the particular requirements of a building site.

Scale Effects

The application of scaled reinforcements distinguishes the current study from the earlier studies. The tensile strength of the geogrids used in the prototype model has been chosen as the most effective parameter because not all of the model parameters can be scaled. The geogrids for physical modeling were chosen according to their amount of stretching under axial loading. The geogrid was chosen for the small-scale model after conducting axial tensile tests on materials with different tensile strengths and then applying scaling rules.

Many studies have examined the behavior of scaled geogrids embedded in soil using techniques such as centrifuge and shaking table tests [39–44] and static loading experiments [7, 12, 23, 45]. Figure 1 shows how the uniaxial tension tests were carried out on the materials using laboratory-scale geogrids. After evaluating the tensile strengths of the scaled (model) and real geogrids (prototype), a scale factor of 1:7.5 was selected for the tests.

Careful efforts were made to verify that the experimental results were dependable and appropriate to real-world situations to precisely address the scaling effect of geosynthetic reinforcement in this study. The ASTM D4595-17.2017 and ASTM D6637/D6637M-15.2015 standards were carefully followed when conducting tensile strength testing on geogrids [46, 47]. A rigorous framework for assessing the mechanical characteristics of the geogrids was supplied by these standards. A key component of the research involved the careful selection of a scale factor of 7.5 to effectively bridge the gap between the reduced-scale model and the real-world field circumstances. The tensile load capacity

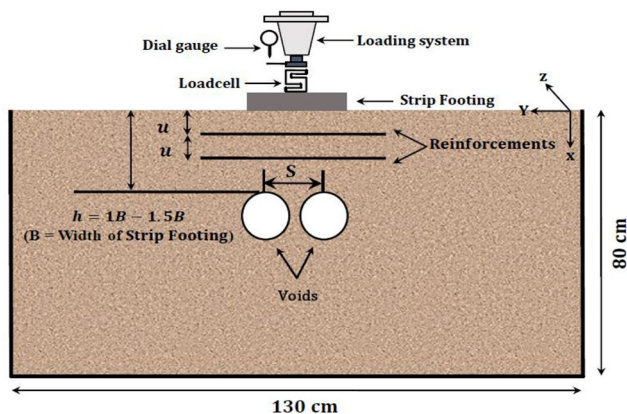


Fig. 1 Schematics of test chamber

and the longitudinal strain at the ultimate load value were the two important parameters to which this scaling factor was applied. This scaling of the parameters was intended to improve the accuracy and consistency of the results by accurately replicating the behavior and interaction of the geogrid reinforcement within the experimental setup.

The general mechanisms and behaviors seen in model tests are successfully reproduced at a larger scale, as shown in large-scale tests conducted by Milligan et al. [48] and Adams and Collin [49]. Therefore, in terms of qualitative analysis, this work offers an insightful understanding of the basic mechanisms controlling the bearing pressure versus settlement responses of sandy beds that have continuous voids reinforced with geosynthetic material. These results will be very helpful in directing large-scale model tests in the future and improving numerical simulation accuracy. Through comprehension of the fundamental concepts, engineers may accurately predict and manage the behavior of reinforced foundations in different scenarios, resulting in safer and more effective designs.

Test Materials

Test Apparatus

A scale factor of 1:7.5 was used when conducting experiments at laboratory scale; thus, all dimensions in this research were divided by 7.5. A chamber with a length of 130 cm, a width of 50 cm and a height of 80 cm was used to make the physical models. Plexiglas was used for the front face of the box to facilitate imaging of the process using the PIV method. In order to ensure that the shape of the Plexiglas did not deform during the experiments, a sheet with a thickness of 3 cm was used. A discharge valve was installed at the rear of the chamber to expedite soil discharge after the experiments. Figure 1 shows a schematic of the test chamber along with the components used in the test.

Soil

Dry sand from the Sufian region of East Azerbaijan province in northwestern Iran was used for all experiments. Various tests were performed on the Sufian sand samples to determine the strength properties and soil parameters. Furthermore, ASTM D3080-04 [50], ASTM D698 [51], ASTM D854 [52], and ASTM D2487 [53] were the standard methods for conducting the direct shear test, compaction test, specific gravity, and soil classification, respectively. The grain-size distribution curve of the soil is shown in Fig. 2. The characteristics of soil resistance and the results are shown in Table 1.

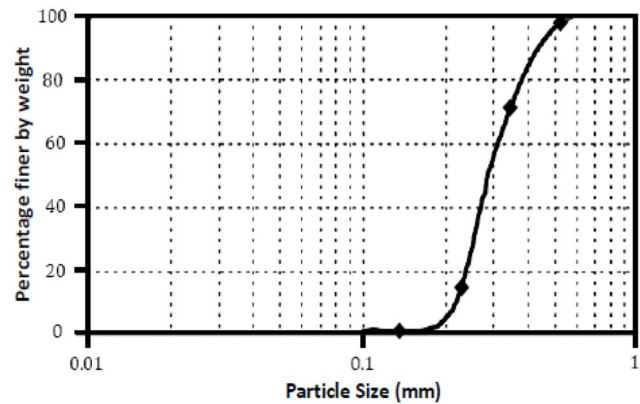


Fig. 2 Grain-size distribution of sand

Table 1 Physical characteristics of soil

Description	Value
Coefficient of uniformity, C_u	1.36
Coefficient of curvature, C_c	0.87
Effective grain size, D_{10} : mm	0.22
Medium grain size, D_{50} : mm	0.28
Maximum void ratio, e_{max}	0.822
Minimum void ratio, e_{min}	0.54
Specific gravity, G_s	2.637
Maximum dry unit weight, γ_{dmax} : kN/m ³	16.76
Minimum dry unit weight, γ_{dmin} : kN/m ³	14.20
Friction angle, ϕ : degree	28
Dry unit weight ($D_r=35\%$): kN/m ³	14.78
Friction angle ($D_r=35\%$), ϕ : degree	32
Dry unit weight ($D_r=73\%$): kN/m ³	15.96
Friction angle ($D_r=73\%$), ϕ : degree	37

Rectangular Footing

The rectangular footing used for loading had a width that was 1 mm smaller than the width of the test tank in order to minimize friction between them and to properly establish plane-strain conditions. A rectangular footing of 49.9 cm in length, 20 cm in width and 3 cm in thickness was used. The surfaces of the rectangular footing were polished to reduce friction to the lowest possible amount.

Voids

Flexible plastic pipes having a diameter of 9 cm and a thickness of 1.8 mm (1.8 = thickness of the pipe material) were used for modeling the soil voids. To prevent friction between the pipes and the tank, the length of the pipes and the length of the rectangular footing were selected to be 49.9 cm, which is 1 mm less than the tank width. The axial and bending stiffnesses of the pipes were disregarded and the pipes were regarded as voids because of their low thickness and low modulus of elasticity.

Table 2 Physical and mechanical properties of scaled geogrids

Type of reinforcement	Material	Opening dimensions (mm)	Thickness (mm)	Extension at failure (%)	Axial load capacity (kN/m)	Elastic modulus (kN/m)
Geogrid	Polypropylene	5×5	1.8	6	2.61	121.2

Table 3 Details of experimental program

Row	Type of reinforcement	Distance between voids (cm)	Geogrid embedment depth (cm)	Vertical spacing between geogrids (cm)	Soil relative density (%)	Number of tests
1	Unreinforced	3 ($S/B=0.6$) 7 ($S/B=0.8$)	-	-	35–73	8
2	1 layer of geogrid ($G1$)	3 ($S/B=0.6$) 7 ($S/B=0.8$)	3.5 ($u3.5$) 7 ($u7$)	3.5-7	35–73	8
3	1 layer of geogrid ($G1$)	3 ($S/B=0.6$) 7 ($S/B=0.8$)	3.5 ($u3.5$) 7 ($u7$)	3.5-7	35–73	8
4	2 layers of geogrid ($G2$)	3 ($S/B=0.6$) 7 ($S/B=0.8$)	3.5 ($u3.5$) 7 ($u7$)	3.5-7	35–73	8
5	2 layers of geogrid ($G2$)	3 ($S/B=0.6$) 7 ($S/B=0.8$)	3.5 ($u3.5$) 7 ($u7$)	3.5-7	35–73	8

Geogrid

Geogrids were used for soil reinforcement at laboratory scale. In all experiments, the length of the geogrid was 50 cm in accordance with the results of a similar study by Moghaddas Tafreshi et al. [23], which showed that the optimal length of a geogrid in their laboratory studies was about 50 cm. Initially, similar tests were performed with geogrids having lengths of 50 cm and 100 cm (5 times the width of the rectangular footing). The bearing capacity of the soil reinforced with the 100-cm geogrid was not significantly different from that of the soil reinforced with the 50-cm geogrid. Therefore, in all experiments, the geogrids used had lengths and widths of 50 cm. Table 2 lists the physical and mechanical characteristics of the geogrids.

Experimental Procedure

The objective of this study was to examine the influence of parameters such as the soil relative density, number of geogrid layers, vertical distance between geogrids in a two-layer configuration, the outer distance between voids (S/B), embedment depth of the voids (h/B) and embedment depth of the first geogrid layer (u). Forty laboratory tests were conducted. Each laboratory test was repeated three times to ensure the accuracy of the results and to confirm the findings. Table 3 lists the specifics of laboratory modeling.

The same construction process was used for every model. This included backfilling, compacting of the soil layers, placement of the pipes and installation of the reinforcements. The tamping of each soil layer and 10-cm backfill layers were done using the same weight to ensure that all soil layers had the same density. The backfilling

and compacting of the soil continued until the pipe placement area was reached. The pipes then were positioned at a heights of 30–40 cm from the container bottom. After the pipes were installed, the soil layers were backfilled and compacted until point at which the reinforcements were installed. After the reinforcements were installed, the final soil layers were poured and a rectangular footing was placed on the sand. The footing featured two strain gauges which were used to control the amount of displacement. A datalogger and a loadcell with a 3-ton load capacity were used to measure the force.

The constant strain loading method was used in order to achieve the greatest accuracy and the same loading rate for all experiments. A displacement of 5 cm was applied in 10 steps of 5 mm. Each test was carried out in 11 stages, where the first stage was without loading and subsequent stages were loading for displacement. In all steps, photographs were taken of the front face of the soil tank to allow for PIV analysis. Figure 3 provides images of the tank and its components.

Test Results and Discussion

Load Bearing Capacity in Loose Soil

Figure 4 shows the load-settlement diagrams for soil reinforced with geogrids positioned above twin voids. The charts and symbols used for every case have been standardized in Figs. 4 and 5 using uniform colors and markers to ensure the graphs' clarity and comparability. The following conditions in these figures are represented by the square, diamond, triangle, circle, and cross markers, in that order:

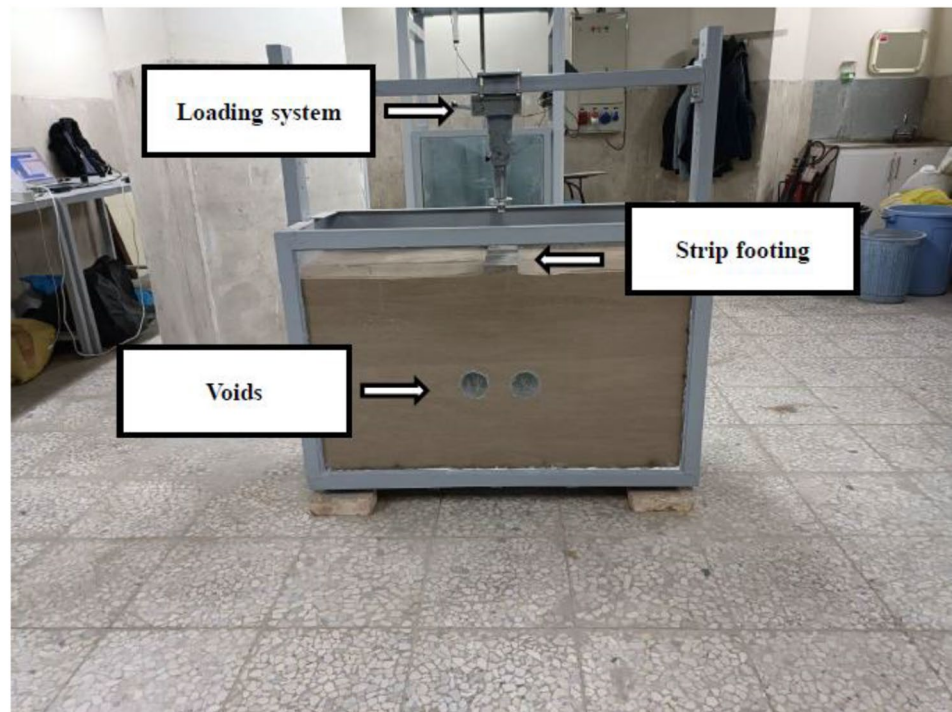
Fig. 3 Tank used for tests with its components: **(a)** datalogger; **(b)** loading jack with strain gauge on foundation; **(c)** front view of tank



(a)



(b)



(c)

Unreinforced soil (*UN*), soil reinforced with one geogrid layer embedded at a depth of 3.5 cm below the soil surface (*G1-u3.5*), soil reinforced with one geogrid layer embedded at a depth of 7 cm below the soil surface (*G1-u7*), soil reinforced with two geogrid layers embedded at a depth of 3.5 cm below the soil surface (*G2-u3.5*), and soil reinforced with two geogrid layers embedded at a depth of 7 cm below the soil surface (*G2-u7*).

Figure 4a shows that the soil reinforced with a single geogrid layer buried at depths of 3.5 and 7 cm from the ground surface increased by 16.5% and 25.1%, respectively, over the unreinforced soil in scenarios where $h/B=1$ and $S/B=0.6$. The addition of two geogrid layers at depths

of 3.5 and 7 cm from the ground surface, the soil bearing capacity increased by 34.9% and 45.1%, respectively, from the previously stated conditions.

The addition of 1 or 2 geogrid layers buried at a depth of 3.5 cm from the soil surface increased the bearing capacity of the reinforced soil by 11% and 30.5%, respectively, compared to the bearing capacity of unreinforced soil with voids at $h/B=1$ and $S/B=0.8$ (Fig. 4b). Similar void placement conditions caused an 18.6% increase in the bearing capacity of the soil reinforced with one geogrid layer at a distance of 7 cm compared to unreinforced soil. A 38.4% increase was observed when two geogrid layers were added at the same depth and spacing.

Fig. 4 Load-settlement diagrams of loose soil with twin voids under different conditions

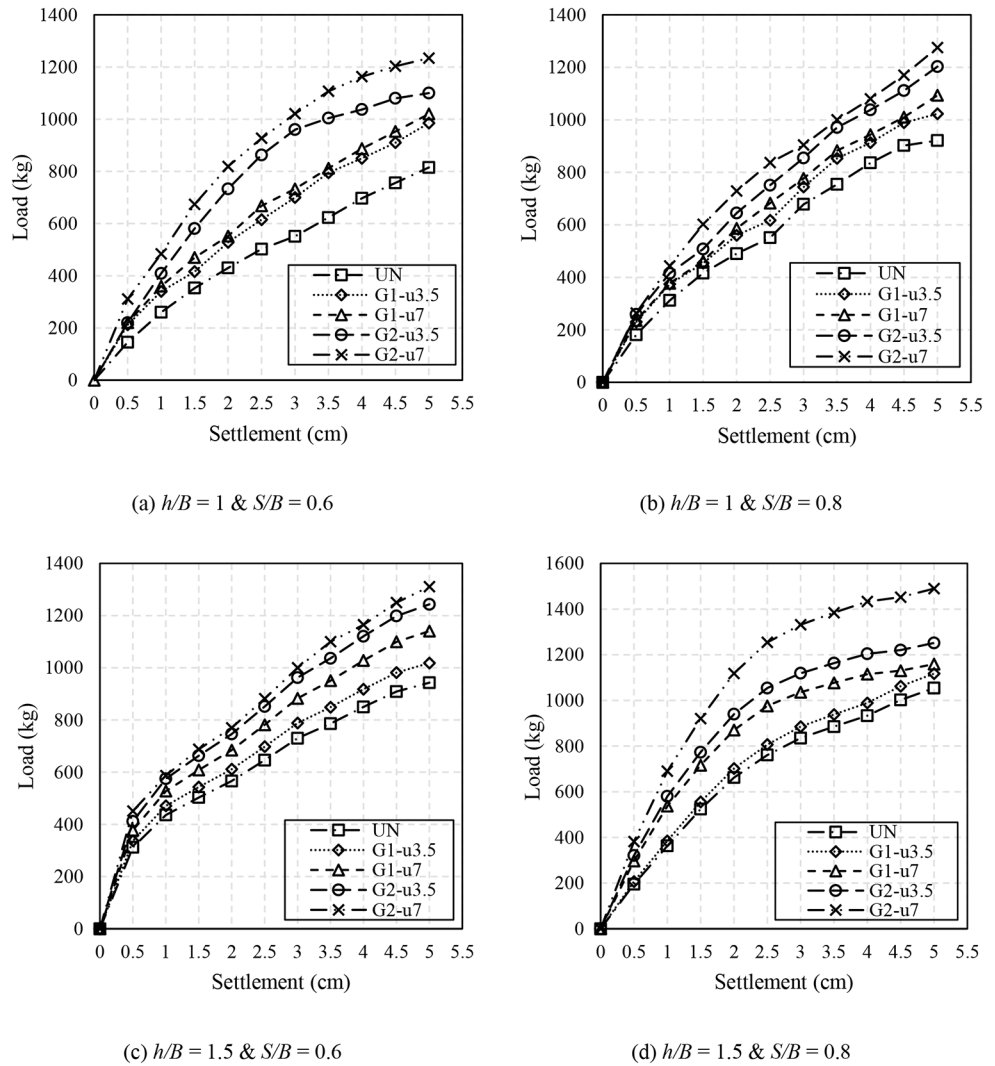


Figure 4c shows that the bearing capacity of soil reinforced with one geogrid layer at depths of 3.5 cm and 7 cm increased by 7.9% and 20.8%, respectively, compared to unreinforced soil at $h/B=1.5$ and $S/B=0.6$. In addition, the bearing capacity of the soil reinforced with two geogrid layers at depths of 3.5 and 7 cm increased by 31.8% and 39%, respectively, in comparison to the soil without reinforcement.

Figure 4d shows that the addition of 1 or 2 geogrid layers buried at a depth of 3.5 cm increased the bearing capacity of the reinforced soil by 5.9% and 18.7%, respectively, compared to unreinforced soil at $h/B=1.5$ and $S/B=0.8$. Soil reinforced with one or two geogrid layers at a burial depth of 7 cm increased the bearing capacity of the reinforced soil by 9.9% and 41.2%, respectively, in comparison with unreinforced soil.

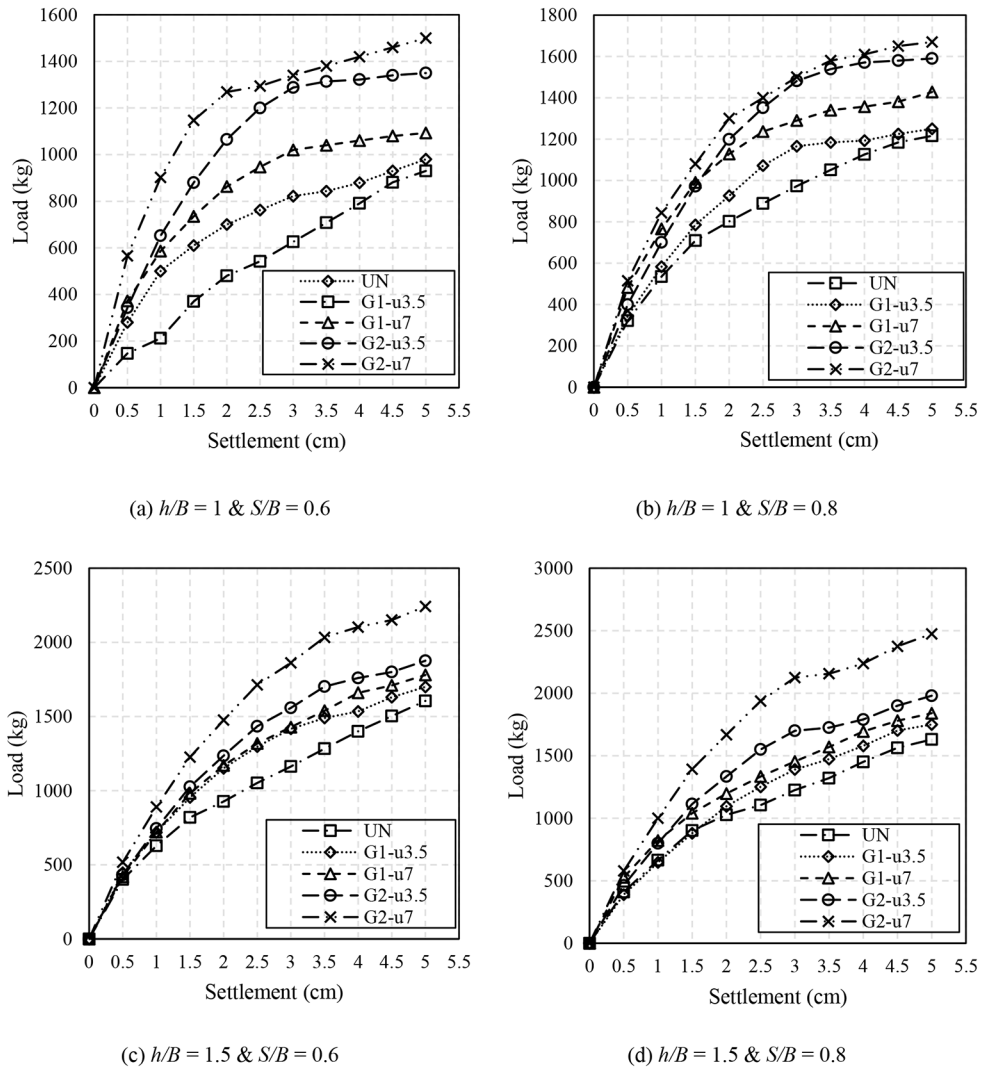
An increase in the S/B from 0.6 to 0.8 at $h/B=1$ and $h/B=1.5$, increased the bearing capacity of loose soil without reinforcements by 13% and 11.7%, respectively. When

$h/B=1$ was increased to $h/B=1.5$, the bearing capacity of the loose unreinforced soil increased by 15.7% at $S/B=0.6$. At $S/B=0.8$, when $h/B=1$ was increased to $h/B=1.5$, the soil bearing capacity increased by 14.4%.

The bearing capacity of the geogrid-reinforced loose soil likely increased as the void ratio increased because the voids spread beyond the area where the loads under the footing affected them. It is also possible that the higher void ratio reduced the interaction between the two voids under the footing, which in turn increased the bearing capacity of the geogrid-reinforced soil.

A higher void embedment ratio was shown to increase the bearing capacity of the geogrid-reinforced soil in the results of experiments carried out in loose soil. Additionally, as the distance of the voids beneath the footing increased along with their embedment ratio, the influence of the voids on the footing bearing capacity decreased, leading to an increase in the soil bearing capacity.

Fig. 5 Load-settlement diagrams of dense soil with twin voids under different conditions



Load Bearing Capacity in Dense Soil

The load-settlement diagrams for dense soil reinforced with geogrids over voids with different h/B and S/B ratios are shown in Fig. 5. The bearing capacity of soil reinforced with one geogrid layer embedded at depths of 3.5 cm and 7 cm increased by 0.3 and 13.8%, respectively, compared to the unreinforced soil shown in Fig. 5a, where the voids were located at $h/B = 1$ and $S/B = 0.6$. The use of two geogrid layers at burial depths of 3.5 cm and 7 cm increased the bearing capacity compared to unreinforced soil with voids by 37.5% and 56.3%, respectively.

With an increase in the S/B ratio to 0.8 at $h/B = 1$, the addition of 1 or 2 geogrid layers buried at a depth of 3.5 cm improved the bearing capacity of the unreinforced soil by 11% and 41%, respectively (Fig. 5b). As the geogrid burial depth reached 7 cm, the bearing capacity increased by 17.9% and 48.3%, respectively, compared to unreinforced soil at $h/B = 2$ and $S/B = 0.8$.

Figure 5c shows that one geogrid layer embedded in the soil with voids at $S/B = 0.6$ and $h/B = 1.5$ and at depths of 3.5 cm and 7 cm increased the soil load bearing capacity by 5.9% and 10.9%, respectively. Under similar conditions, the increase in soil bearing capacity with 2 geogrid layers at depths of 3.5 cm and 7 cm was 16.8% and 39.6%, respectively, compared to unreinforced soil.

Figure 5d shows that the bearing capacity of unreinforced soil compared to soil reinforced with 1 or 2 geogrid layers at a burial depth of 3.5 cm was 7.3% and 21.4%, respectively, at $h/B = 1.5$ and $S/B = 0.8$. Additionally, compared to unreinforced soil, the bearing capacity of soil reinforced with one or two geogrid layers at a buried depth of 7 cm increased by 12.8% and 51.8%, respectively.

In unreinforced soil, an increase in S/B from 0.6 to 0.8 resulted in an increase in the soil bearing capacity of 17.2% and 1.5%, respectively, at $h/B = 1$ and $h/B = 1.5$. An increase in from $h/B = 1$ to $h/B = 1.5$ increased the soil load bearing

capacity in compacted unreinforced soil by 67.1% for voids at $S/B=0.6$ and 44.7% for voids at $S/B=0.8$.

The soil layer between the footing and the void became thinner as the voids were located closer to the footing and had a lower embedment ratio (h/B). The soil experienced a decrease in shear strain prior to failure as a result. Their negative effects decreased and the bearing capacity increased when h/B increased [23]. Previous research has shown that there is a positive correlation between an increase in soil arching and a decrease in the effect of the void on the soil bearing capacity, which increases the shear resistance [34, 54]. With the failure of plane arching, h/B increased the soil shear resistance. As a result, the layer of soil above the voids that was reinforced with a geogrid carried a larger proportion of the load and the voids carried a smaller percentage of the load [23].

The surcharge above the first geogrid layer increased when the embedment depth increased to 7 cm ($u/B=0.35$). This increased the bearing capacity of the geogrid-reinforced soil because it increased the frictional resistance between the geogrid and the sand. A study by Tafreshi and Khalaj [5] showed that the soil layer between the reinforcement and the footing produced less surcharge that would create frictional resistance between the sand and the geogrid at the sand-reinforcement interface when $u/B < 0.35$. Previous research by Tafreshi et al. [10] suggested an optimum embedment depth of $0.25D$ to $0.4D$ (D =diameter of the circular footing) for single-layer geosynthetic reinforcements located below the circular footings. This depth promoted the formation of external arching below the footing, mobilizing the tensile capacity of the geosynthetics and enhancing the bearing capacity. Other studies have similarly stated that an increase in the u/B ratio of reinforcements beyond 0.35 reduced the effectiveness of the reinforcement and lowered the bearing capacity of the geogrid-reinforced soil [55, 56].

The shear resistance and load distribution in the system will increase as the number of geogrid layers increases above the void. The risk of instability and collapse of the void will decrease when the load transferred to the void crown decreases with an increase in the stiffness and shear resistance [23]. Previous investigations have revealed that an effect resembling soil arching occurs with the addition of more layers of geosynthetic reinforcement [54, 57] which reduces the load imposed on the void, increasing its stability [23]. Moghaddas Tafreshi et al. [23] also reported that increasing the number of reinforcement layers had a substantial effect on the strain that developed along the geogrid length as well as on the bearing capacity of the soil reinforced by the geogrid. The internal confinement effect proposed by Yang [58] may be the cause of this phenomenon.

The internal confinement effect is related to the level of friction at the soil-reinforcement interface, the tensile

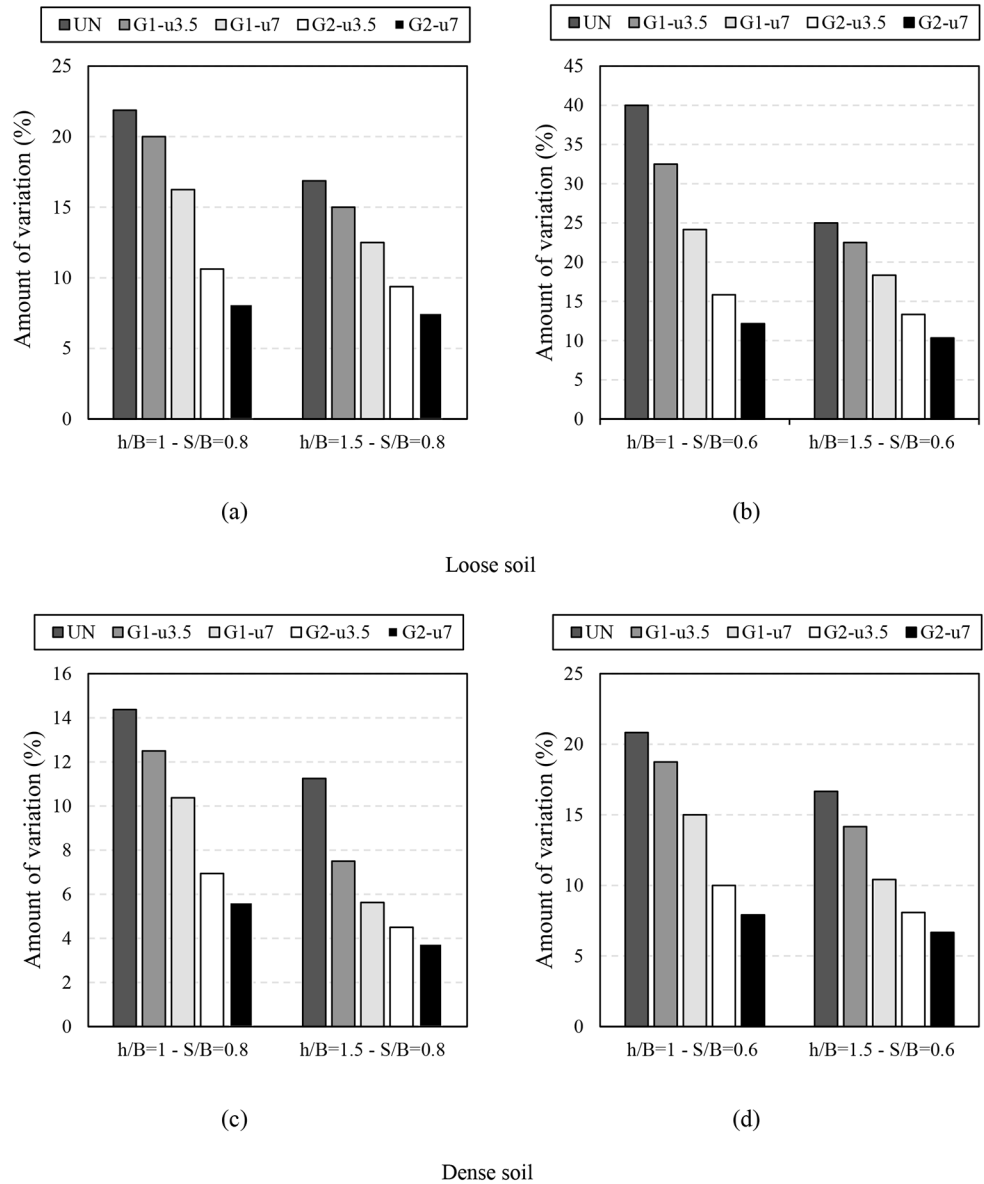
strength of the reinforcement and the confining stress that develops on the backfill soil in the geogrid apertures as a result of the passive resistance provided by the geogrid [23, 59]. An increase in soil density will cause more soil to be deposited above the void, which will cause the load to be distributed more uniformly over the void and decrease the load transferred to the void crown. Compacted reinforced sand layers perform better when the overburden on top of the void increases and permits greater shear strain to be sustained before failure, preventing direct soil penetration between the footing and the void [23].

Horizontal Displacement of Voids

The change in the horizontal distance between voids with respect to the original value (S) was investigated and the results are displayed as a percentage (%) in Fig. 6. In Fig. 6, the results of all experiments with similar characteristics have been presented in the same color to make it easier to compare different cases. For example, the results of tests performed without reinforcement are displayed in black in the corresponding bar chart. In the bar graphs, the results of tests performed on voids with a constant S/B ratio are represented by the horizontal axis, while the variations in the parameter S are indicated by the vertical axis. The voids in the unreinforced loose soil at $h/B=1$ and $S/B=0.6$ experienced the greatest change in the horizontal distance between them (40%). This change in the horizontal distance between the voids at $h/B=1$ and $S/B=0.6$ decreased to 20.8% with an increase in the density of the unreinforced soil, which indicates that there was fewer volume of the gaps between the soil particles in the unreinforced condition as soil density increased. As a result, less soil particle migration occurred between and above the voids. Reduced soil particle displacement resulted in less soil pressure being applied to the voids during loading, which reduced the amount of displacement between the voids.

A decrease in the horizontal distance between voids was observed in all instances where the void embedment ratio (h/B) increased from 1 to 1.5. This occurred because the soil particles received a greater proportion of the loading-induced displacement when more soil was deposited above the voids. The horizontal distance between the voids showed a smaller increase at $h/B=1.5$ than at $h/B=1$. Additionally, the rate of change in the horizontal distance between the voids decreased as S/B increased from 0.6 to 0.8. The increase in the soil volume between the voids decreased the portion of the load that reached the voids because more soil was deposited between them and caused the void distance ratio to increase. Horizontal displacement of the voids also decreased as the load on them increased. In this case, as the soil density increased, the internal friction angle of the soil

Fig. 6 Percentage of change in horizontal space between voids under different conditions



particles also increased. It was more apparent in the tests on compacted soil that the interlock between the soil particles became stronger as the internal friction angle of the soil particles increased, resulting in a decrease in soil particle displacement.

Analysis of the experimental results indicated that the use of a geogrid to reinforce the soil considerably reduced deformation caused by loads applied to the foundation. Increasing the number of geogrid layers above the voids improved the shear resistance and stiffness of the geogrid-reinforced soil, which in turn increased the bearing capacity and reduced particle movement under loading. Changes in the horizontal distance between voids decreased with a decrease in particle displacement. Figure 6 demonstrates that the change in the horizontal distance between voids at $S/B=0.8$ was 5.6% and 3.7% for voids at $h/B=1$ and

$h/B=1.5$, respectively, for compacted soil reinforced with two geogrid layers embedded at a distance of 7 cm from the ground surface.

The overburden on the reinforcements increased as the embedment depth of the first geogrid layer increased from 3.5 to 7 cm. Friction between the soil and the reinforcements increased as the overburden on them increased. Particle displacement between the voids decreased with an increase in the soil-reinforcement friction. The increased shear resistance and improved soil particle interlock of the system were the causes of this decrease and resulted in less change in the horizontal distance between the voids.

Fig. 7 Geogrid used in physical modeling: **(a)** before testing; **(b)** after testing

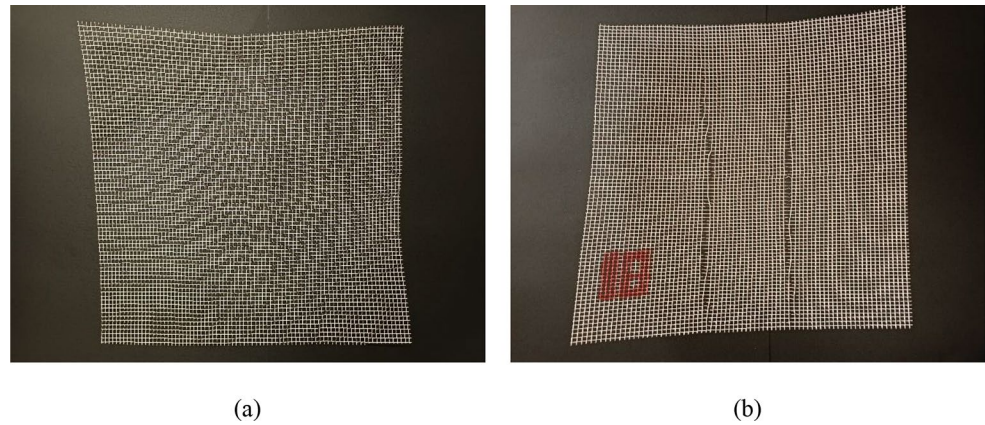


Table 4 Maximum measured length of geogrid aperture under different conditions (mm)

Row	Soil density	Loose				Dense				
		Embedment ratio of voids		Embedment ratio of voids		Embedment ratio of voids		Embedment ratio of voids		
		h/B = 1		h/B = 1.5		h/B = 1		h/B = 1.5		
	Number and embedment depth of geogrid	Distance ratio of voids								
		S/B = 0.6	S/B = 0.8	S/B = 0.6	S/B = 0.8	S/B = 0.6	S/B = 0.8	S/B = 0.6	S/B = 0.8	
1	G1-u3.5	19.2	17	15.7	15.4	18.3	16.5	14.5	14.1	
2	G1-u7	16.9	15.8	14.9	13.5	16.2	15.6	12.8	12.3	
3	G2-u3.5	Upper layer	15.9	14.6	13.5	12.6	14.9	14.1	12	11.5
		Lower layer	15.3	13.2	12.5	11.1	14.2	11.2	10.6	10.2
4	G2-u7	Upper layer	12.9	11.8	10.8	10.1	13.8	10.5	10	9.1
		Lower layer	12.1	11.3	10	9.7	12	9.8	9	8.2

Change in Dimensions of Geogrid Apertures

A caliper was used to measure changes in the geogrid apertures to investigate the effect of loading on a footing placed on soil reinforced with geogrids. Figure 7 shows a sample of the geogrid used before and after testing. After testing, it was found that the length of the geogrid apertures increased in an area that was almost equivalent to the footing width (B) when loading was applied. The tensile forces in the reinforcements were mobilized as a result of loading. An increase in aperture elongation in the reinforcements and the risk of reinforcement rupture occurred when the mobilized tensile force exceeded the ultimate tensile strength of the geogrid.

Table 4 displays the maximum extent of elongation caused by loading in the geogrid apertures as measured by calipers. The single geogrid layer embedded at a depth of 3.5 cm ($G1-u3.5$) in loose soil with voids ($h/B = 1$ and $S/B = 0.6$) showed the greatest increase in geogrid aperture length. Several geogrid apertures in the areas corresponding to the footing width grew to a length that was 3.84 times greater than the original length (5 mm). The dense soil with voids and two geogrid layers embedded at a depth of 7 cm ($G2-u7$; $h/B = 1.5$ and $S/B = 0.8$) showed the least increase in geogrid aperture length. In that case, the geogrid apertures in areas matching the footing width showed a 1.64-fold increase in length.

The data shows that the increase in the geogrid aperture length decreased progressively as the embedment depth of the initial geogrid layer increased in every scenario. It appeared that more of the load was transferred to the soil above the reinforcement than to the reinforcement itself as the height of the soil overburden imposed on the reinforcement increased. In this case, as the embedment depth of the first geogrid layer increased, the change in the length of the geogrid apertures decreased. The geogrids embedded at shallower depths experienced greater tensile force than geogrids embedded at lower depths. In contrast to the geogrids embedded at lower depths, the increase in the length of the geogrid apertures embedded at shallower depths was more noticeable.

As the number of geogrid layers increased, the increase in the length of the geogrid aperture in the reinforcement with two geogrid layers was observed to be considerably less than that of the reinforcement with one geogrid layer. Placement of the reinforcements within the effective depth of reinforcement increased the soil lateral confinement, which increased the system load-bearing capacity and decreased deformation in the geogrid-reinforced soil system. It also was noted that, as the number of geogrid layers and the embedment depth increased, the load distribution increased and less load was transferred to the second geogrid layer and, ultimately, to the voids.

The analysis suggests that an increase in the soil density caused a decrease in the change of length in the geogrids. The volume of voids in the soil decreased and soil density increased, which brought the soil particles closer together. The load distribution among the soil particles became more significant and uniform as the soil particles became closer together. The densification of the soil resulted in a decrease in system deformation and an increase in the system load-bearing capacity.

PIV Results

Particle image velocimetry (PIV) was used to assess how the parameters under study affected the occurrence of failure wedges and the amount of strain at the slip surface. Figures 8, 9, 10, 11 and 12 display the findings of image analysis carried out under different conditions. The range of shear strain is shown in the images in the right column of each figure. The shapes on the left represent tests carried out in dense soil and the shapes on the right represent tests carried out in loose soil.

Figure 8 shows that failure wedges were generated in the Rankine passive zones having the largest shear strain and extended to the ground surface in loose soil without reinforcement ($h/B = 1$ and $S/B = 0.6$) as a result of the pressure imposed on the footing. The range of shear strain on the failure wedges were at a maximum in this test. The magnitude of the shear strain at the intersection of the voids and the Rankine passive zones decreased when S/B increased from 0.6 to 0.8 in loose soil without reinforcement. In the unreinforced tests, the failure wedge in the Rankine passive zones did not fully form when h/B increased. It is noteworthy that the strain rates were greater for voids at $S/B = 0.6$ than for voids at $S/B = 0.8$ on the slip surface of the Rankine passive zones. Furthermore, in tests conducted in loose soil, the strain was larger than in tests carried out in dense soil on the slip surface in the Rankine passive zone. Because the stiffness and shear strength of loose soil without reinforcement are lower than those of dense soil, larger shear stresses will occur when a load is applied to the footing in loose soil. The generation of larger shear stresses in the soil beneath the footing causes the development of higher shear strains on slip surfaces, suggesting that conditions of loose soil have higher stress concentrations. Moreover, applying a load to the foundation causes the soil beneath it to compress (the Rankine active zone). This compression causes the surrounding soil (the Rankine passive zone) to experience lateral pressure, which causes it to compress and move as well. Because of the aforementioned factors, Rankine passive zones also develop in loose soil conditions.

The strain rates formed in the Rankine passive zones decreased with the use of one geogrid layer as reinforcement

of soil with voids at $h/B = 1$ beneath the footing. Comparison of Figs. 9 and 10 with the results in Fig. 8 shows that the addition of reinforcement to the soil beneath a footing increased the system load-bearing capability and reduced the strain in the system compared to the unreinforced tests. In contrast to test results under similar void conditions without reinforcement, the dense soil with voids at $h/B = 1$ and $S/B = 0.6$ that was reinforced with one geogrid layer at a depth of 7 cm ($G1-u7$) showed a greater decrease in the strain rate in the Rankine passive zones. As the h/B increased from 1 to 1.5, the shear strain in the Rankine active zone in tests with one geogrid layer was less than for similar tests without reinforcement. This was because the dense soil reinforced with geogrid exhibited greater shear resistance than loose soil without reinforcement. When a single geogrid layer is added to the soil beneath the footing, it becomes stiffer and more rigid than it would be in the absence of reinforcement. Additionally, this increases the friction between the soil and the reinforcement, which reduces soil particle movement and the development of shear stresses in the soil beneath the footing. The lateral pressure on the Rankine passive zones decreases as a result of the decreased stresses in the soil beneath the footing. Consequently, there is a reduction in the rate at which shear strain is created in these regions.

The addition of two geogrid layers to the soil beneath a footing prevented the formation of Rankine passive zones owing to the improved load-bearing capability of the system. This could be observed by comparing Figs. 11 and 12 with Figs. 8, 9 and 10. In Figs. 11 and 12, two geogrid layers were used in dense soil with voids at $h/B = 1.5$ and $S/B = 0.8$. The shear strain rate in the Rankine active zone beneath the footing was significantly lower than under the same conditions with one geogrid layer and without a geogrid. The shear strain rate around the voids decreased when two geogrid layers were added to the soil beneath the footing. The lateral confinement or internal confinement between the reinforcement and soil particles was the reason for the decrease in the shear strain rates on the Rankine active zone and around the voids. Because the soil reinforced with geogrids had a higher load-bearing capacity, the strain in the system decreased as the lateral confinement increased. The lateral confinement between the particles of sandy soil is greatly improved by increasing the number of geogrid layers from 1 to 2. Because of the greater lateral confinement, there is less mobility of the sand particles because of the higher friction between them. The stresses that have built up in the soil beneath the footing also lessen when particle mobility declines. As a result of this stress reduction, the soil beneath the footing exerts less lateral pressure on the Rankine passive zones. As a result, soil particle mobility in the Rankine passive zones is restricted due to the decreased lateral pressure in these zones. Consequently, there is a

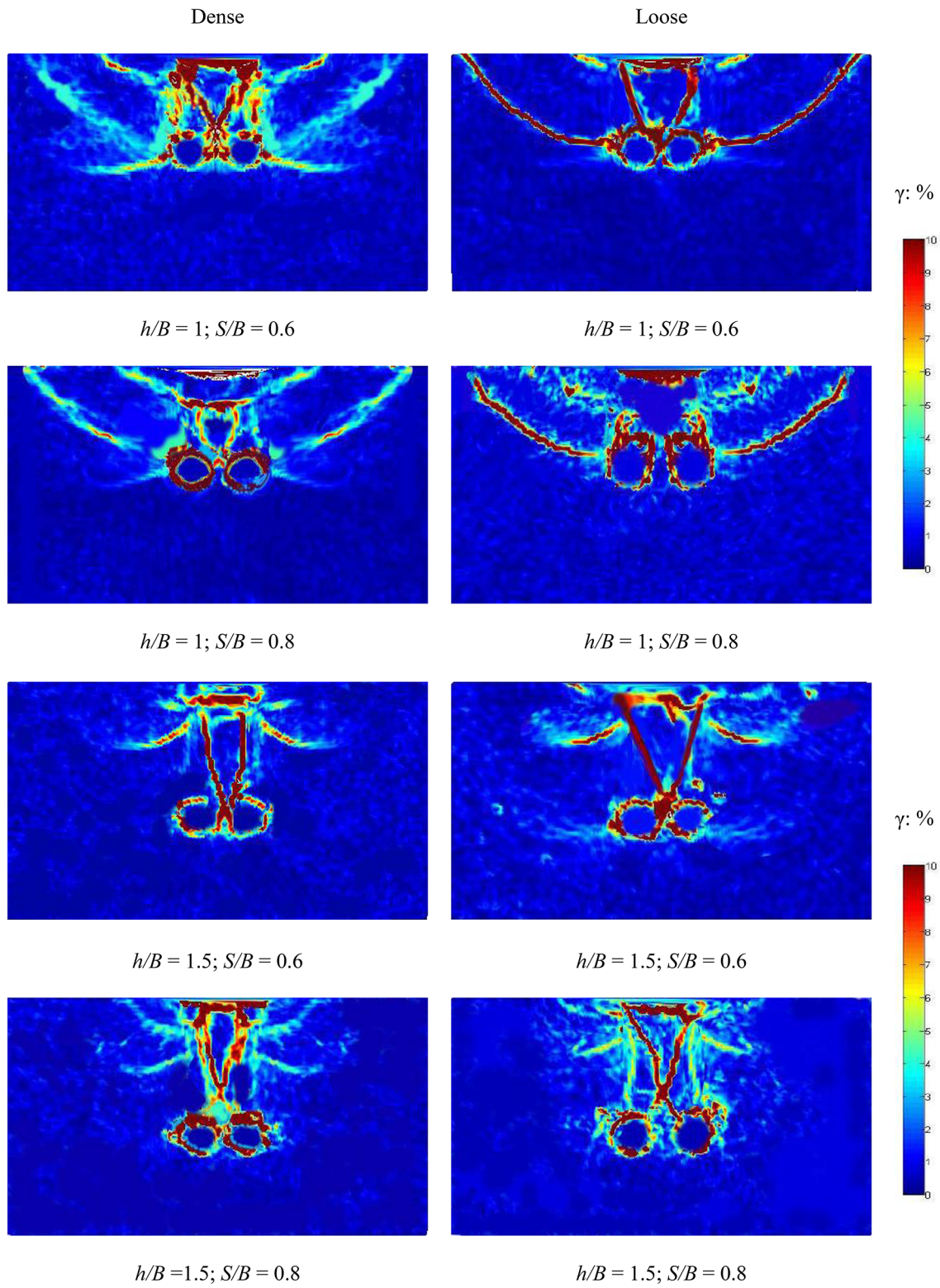


Fig. 8 PIV results for tests performed on unreinforced soil

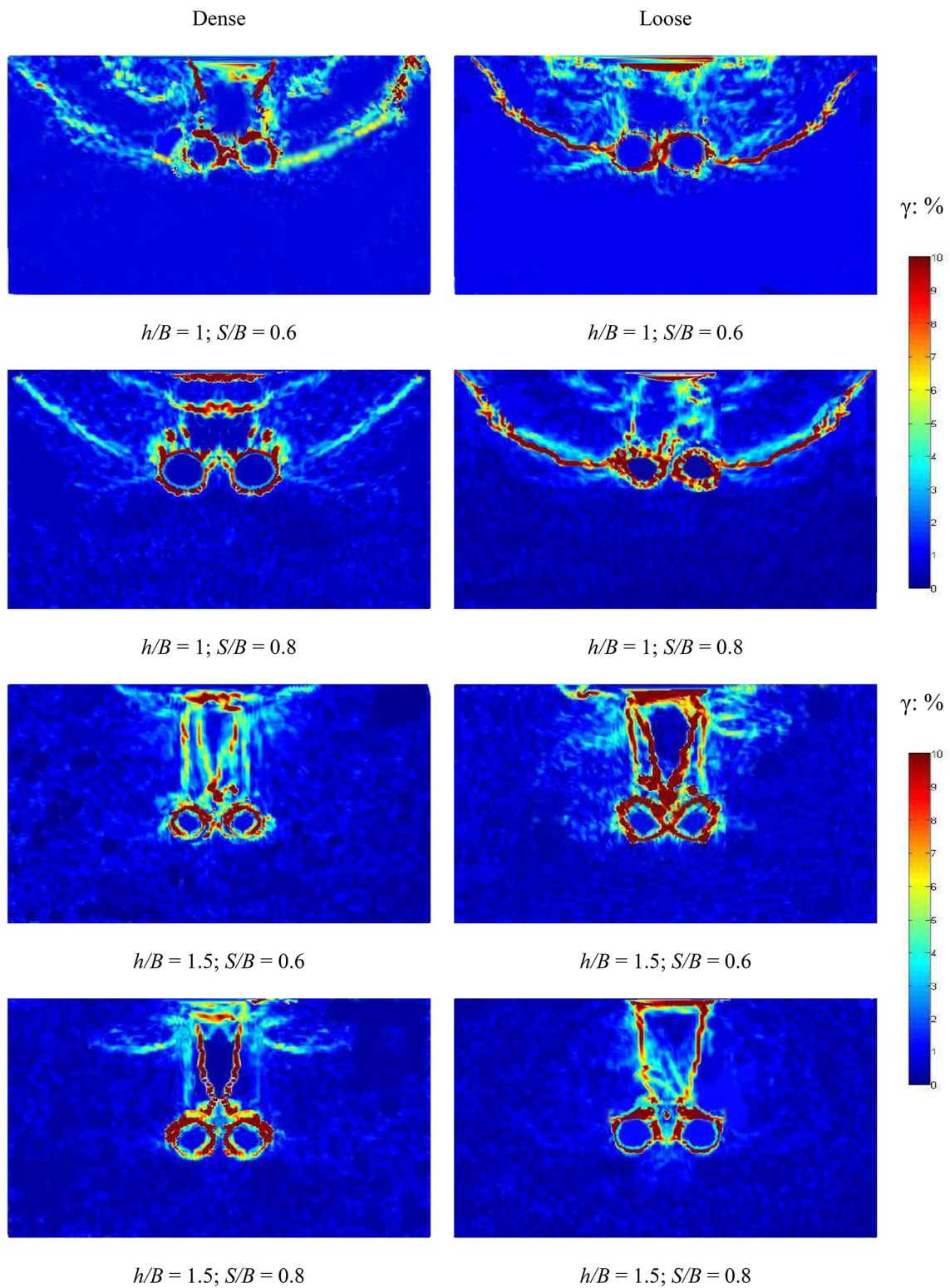


Fig. 9 PIV results for tests performed on soil with 1 geogrid layer embedded at a depth of 3.5 cm (*G1-u3.5*)

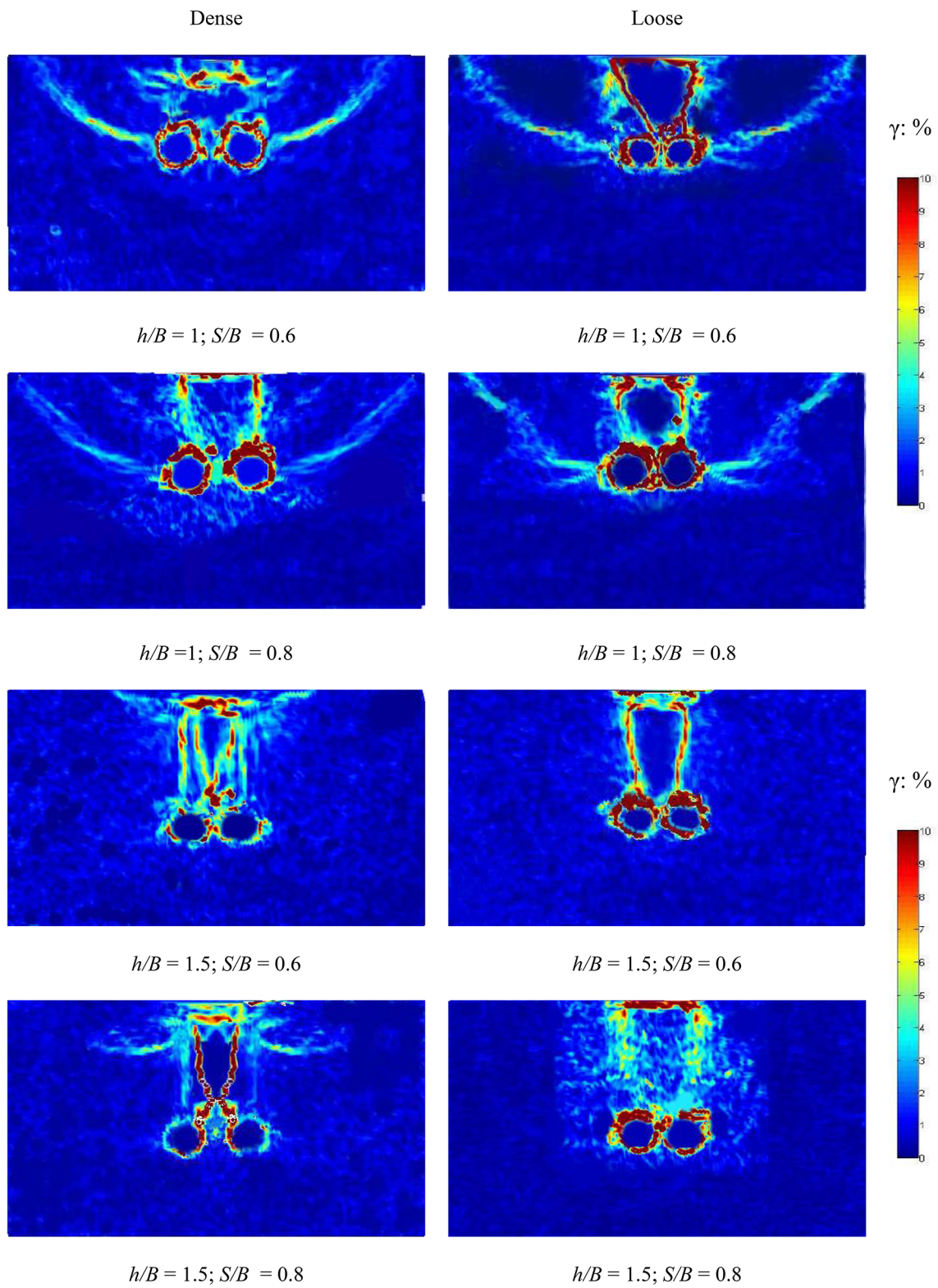


Fig. 10 PIV results for tests performed on soil with 1 geogrid layer embedded at a depth of 7 cm (*G1-u7*)

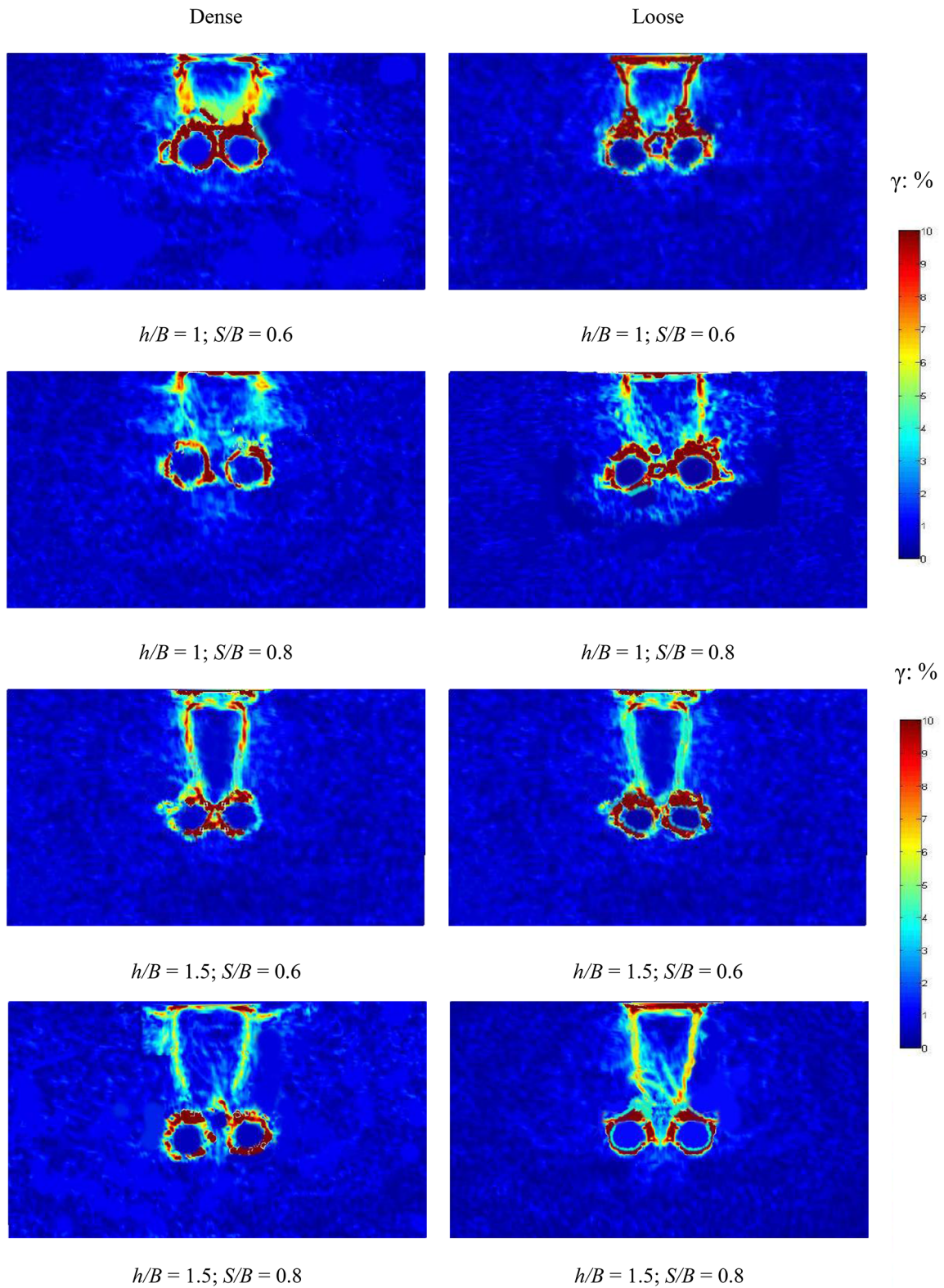


Fig. 11 PIV results for tests performed on soil with 2 geogrid layers embedded at a depth of 3.5 cm (G2-u3.5)

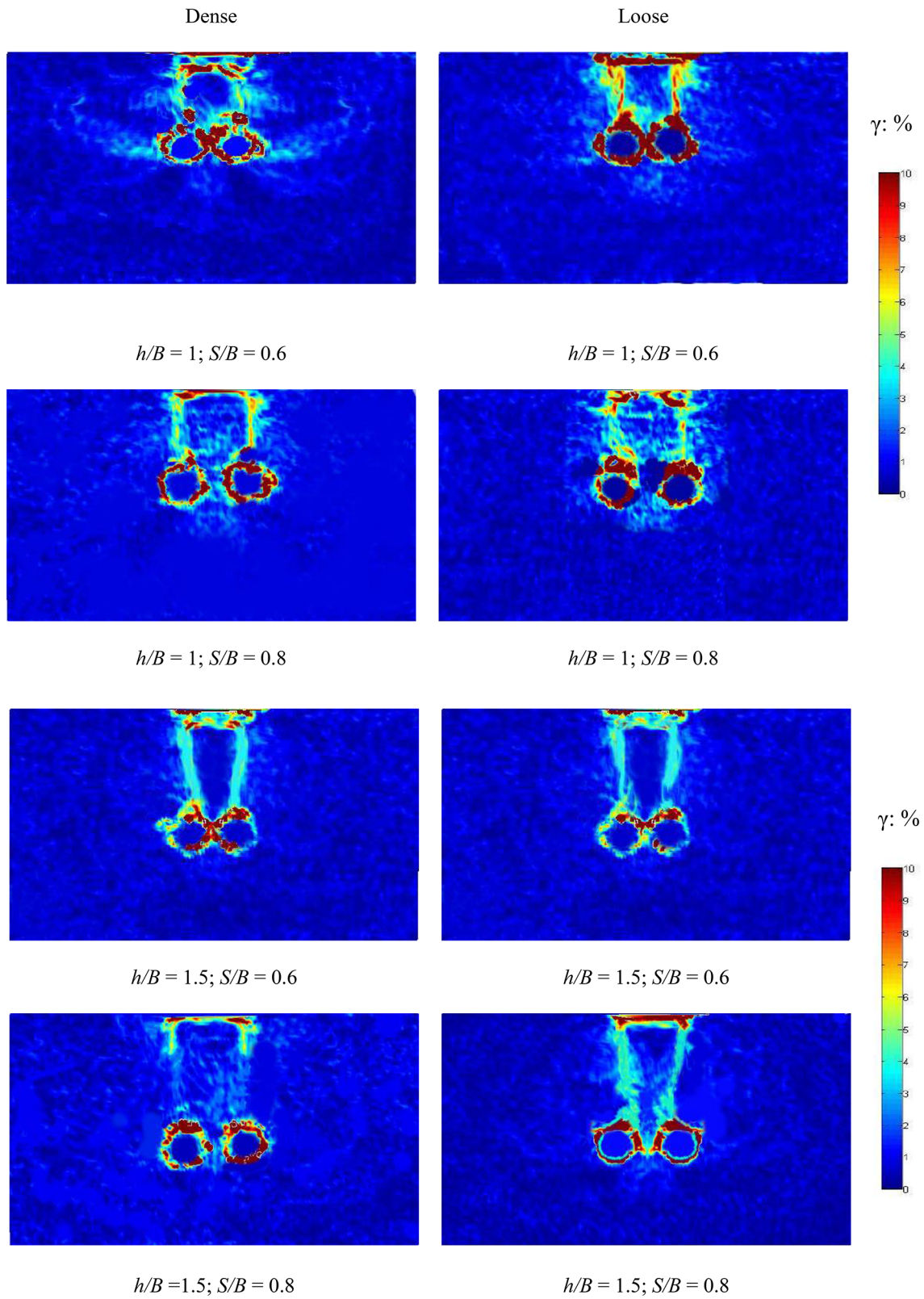


Fig. 12 PIV results for tests performed on soil with 2 geogrid layers embedded at a depth of 7 cm (G2-u7)

significant decrease in strains, especially shear strains, where the slip surface is located.

The PIV results showed that punching shear failure was observed beneath the footing in all tests carried out on soil with voids at $h/B = 1.5$. In tests carried out on soil with and without a single geogrid layer over voids at $h/B = 1$, Rankine passive zones were observed in the soil beneath the footing and the failure type was general shear failure. The zone beneath the footing and the geogrids experienced compression due to the development of general shear failure.

A similarity has been found between the reported failure surfaces in the soil beneath the footing in the current investigation and the numerical study conducted by Kumar and Chauhan [14] based on the examination of PIV data. The failure planes resulting from the interaction between the footing and the voids are curved in both studies, and two more failure planes extend from the apex of both voids to the horizontal ground surface. As noted by Kumar and Chauhan [14], notable shear strains will develop at the apex of twin circular voids if they are located close to the footing. This is because the apex of the voids and the failure planes beneath the footing will intersect, as confirmed in the current investigation. Additionally, Kumar and Chauhan [14] reported that as the horizontal distance between the voids increases, there is less interaction between the voids and the footing, which lowers the shear strain rates that are created, especially at the top of the voids. Similarly, in the current study, shear strain rates developed on the failure surfaces and at the void apex reduced when the S/B ratio of the voids increased from 0.6 to 0.8.

This study's PIV analysis results, when compared to the numerical analysis carried out by Zhao et al. [15], show that symmetrical failure would occur in the soil beneath the footing when circular voids are placed in unreinforced soil. Underneath the footing and above the void, the failure wedges will form symmetrically with identical shear strain rates. Furthermore, it can be claimed that the failure shape for twin circular voids observed in this study is similar to the failure shape for a single circular void that was seen in the aforementioned numerical study. The apex of the void is impacted by the depth of the failure wedges in this type of observed failure. Notably, the failure observed in this study is consistent with scenarios in which the voids are located in the upper regions of the area affected by the load applied on the footing and have a lower embedment ratio ($h/B = 1$).

According to the evaluation and comparison of the PIV analysis results with the findings of the study conducted by Ates and Sadoglu [16], which examined the bearing capacity of sandy soil reinforced with geotextile, the failure wedges found in unreinforced soil and soil with a single reinforcement layer were consistent with earlier theories of bearing capacity (Terzaghi, 1943). The soil has a tendency to move

downward in this type of failure within the wedge beneath the footing, applying lateral pressure to the nearby soil.

Conclusions

The current study examined the behavior of soil with twin voids with and without reinforcement by performing a total of 40 tests on unreinforced sand and sand reinforced with geogrids. The factors assessed were the soil density, the number and spacing of the geogrid layers, their embedment depth and the horizontal spacing of the voids. The results of this investigation showed that:

- The lateral displacement of the voids decreased and the bearing capacity increased with an increase in the S/B of the voids in all scenarios.
- The bearing capacity increased and the lateral displacement of the voids decreased in all tests as the embedment depth ratio of the voids increased.
- The bearing capacity of geogrid-reinforced soil increased significantly as the number of layers increased because of the increase in resistance of the soil beneath the footing. The test results indicated that the bearing capacity of dense soil reinforced with geogrids increased by 51.8% in comparison to unreinforced soil. Among all tests, the two-layer geogrid ($G2-u7$) demonstrated the greatest improvement in bearing capacity.
- In every scenario, an increase in the bearing capacity and a decrease in the lateral displacement of the voids were noted as the soil density increased from 35 to 73%. The system bearing capacity increased with an increase in the soil density because the volume of the gaps in the soil decreased and increased the particle-to-particle friction.
- There was an increase in the frictional resistance between the sand and the geogrid when the embedment depth of the initial layer increased from 3.5 cm to 7 cm. As a result, the lateral displacement of the voids decreased and the system bearing capacity increased.
- The results of PIV analysis indicated that, as the number of geogrid layers and the embedment depth of the upper geogrid layer increased, the rate at which shear strain was generated in the Rankine active zone decreased and Rankine passive zones did not form.
- In tests using two geogrid layers ($G2-u7$), the rate at which the shear strain was generated around the voids in dense soil at $h/B = 1.5$ was much lower than for the other scenarios analyzed. The higher shear resistance of the soil-geogrid system was the reason for this decrease.
- The use of two geogrid layers spaced 7 cm apart ($G2-u7$) is recommended as the ideal condition at laboratory

scale to improve the soil bearing capacity and decrease deformation and displacement brought on by loading of the soil.

Author Contributions Michael Kazemzadeh: Investigation- Resources-Conducting Experiments -Writing – review & editing. Pantea Pezeshkian Investigation- Resources-Conducting Experiments, Resources. Amirali Zad: Conceptualization, Methodology, Resources, Writing – review & editing. Maryam Yazdi: Conceptualization, Methodology, Resources, Writing – review & editing.

Funding The authors declare that no funds, grants, or other support were received during the preparation of this manuscript.

Data Availability The data obtained from experiments are in the Results and Discussion section. If more detail is required about the laboratory results, we can send an excel file.

Code Availability Not applicable.

Declarations

Competing Interests The authors have no relevant financial or non-financial interests to disclose.

References

1. Abu-Farsakh M, Chen Q, Sharma R (2013) An experimental evaluation of the behavior of footings on geosynthetic-reinforced sand. *Soils Found* 53(2):335–348
2. Khing K et al (1993) The bearing-capacity of a strip foundation on geogrid-reinforced sand. *Geotext Geomembr* 12(4):351–361
3. Kou Y, Shukla SK, Mohyeddin A (2018) Effect of width of geosynthetic reinforcement within the granular cover on the load distribution over the tunnel lining. in *Civil Infrastructures Confronting Severe Weathers and Climate Changes Conference*. Springer
4. Yetimoglu T, Wu JT, Saglamer A (1994) Bearing capacity of rectangular footings on geogrid-reinforced sand. *J Geotech Eng* 120(12):2083–2099
5. Tafreshi SM, Khalaj O (2008) Laboratory tests of small-diameter HDPE pipes buried in reinforced sand under repeated-load. *Geotext Geomembr* 26(2):145–163
6. Tafreshi SM, Dawson A (2010) Behaviour of footings on reinforced sand subjected to repeated loading—comparing use of 3D and planar geotextile. *Geotext Geomembr* 28(5):434–447
7. Tafreshi SM, Dawson A (2012) A comparison of static and cyclic loading responses of foundations on geocell-reinforced sand. *Geotext Geomembr* 32:55–68
8. Mehrjardi GT, Tafreshi SM, Dawson A (2012) Combined use of geocell reinforcement and rubber–soil mixtures to improve performance of buried pipes. *Geotext Geomembr* 34:116–130
9. Khalaj O et al (2016) Cyclic Response of Footing with Embedment Depth on Multi-Layered Geocell-Reinforced Bed. in *IOP Conference Series: Earth and Environmental Science*. IOP Publishing
10. Tafreshi SM, Sharifi P, Dawson A (2016) Performance of circular footings on sand by use of multiple-geocell or-planar geotextile reinforcing layers. *Soils Found* 56(6):984–997
11. Chen J et al (2021) Physical and numerical modelling of strip footing on geogrid reinforced transparent sand. *Geotext Geomembr* 49(2):399–412
12. Majidi A, Yazdi M (2023) Physical modeling of the Effect of using scaled Geosynthetic reinforcements on bearing capacity and settlement of Strip Footing. *Int J Geomech* 23(7):04023093
13. Bhattacharya P, Shiau J, Barole S (2021) Improvement of bearing capacity of footings using reinforced granular trench. *Int J Geosynthetics Ground Eng* 7:1–14
14. Kumar P, Chauhan VB (2024) Behavior of footing resting above Dual Circular Cavities in a Rock Mass: insights from an AFELA Study. *Int J Geomech* 24(1):04023248
15. Zhao L et al (2021) Study on the ultimate bearing capacity of a strip footing influenced by an irregular underlying cavity in karst areas. *Soils Found* 61(2):259–270
16. Ates B, Sadoglu E (2023) A quasi-2D exploration of optimum design settings for geotextile-reinforced sand in assistance with PIV analysis of failure mechanism. *Geotext Geomembr* 51(3):418–436
17. Baus R, Wang M (1983) Bearing capacity of strip footing above void. *J Geotech Eng* 109(1):1–14
18. Wang M, Badie A (1985) Effect of underground void on foundation stability. *J Geotech Eng* 111(8):1008–1019
19. Dash SK, Krishnaswamy N, Rajagopal K (2001) Bearing capacity of strip footings supported on geocell-reinforced sand. *Geotext Geomembr* 19(4):235–256
20. Dash S, Rajagopal K, Krishnaswamy N (2004) Performance of different geosynthetic reinforcement materials in sand foundations. *Geosynthetics Int* 11(1):35–42
21. Latha GM, Murthy VS (2007) Effects of reinforcement form on the behavior of geosynthetic reinforced sand. *Geotext Geomembr* 25(1):23–32
22. Sireesh S, Sitharam T, Dash SK (2009) Bearing capacity of circular footing on geocell–sand mattress overlying clay bed with void. *Geotext Geomembr* 27(2):89–98
23. Moghaddas Tafreshi S, Khalaj O, Halvae M (2011) Experimental study of a shallow strip footing on geogrid-reinforced sand bed above a void. *Geosynthetics Int* 18(4):178–195
24. Kiyosumi M, Kusakabe O, Ohuchi M (2011) Model tests and analyses of bearing capacity of strip footing on stiff ground with voids. *J Geotech GeoEnviron Eng* 137(4):363–375
25. Sitharam T, Hegde A (2013) Design and construction of geocell foundation to support the embankment on settled red mud. *Geotext Geomembr* 41:55–63
26. Asakereh A, Ghazavi M, Tafreshi SM (2013) Cyclic response of footing on geogrid-reinforced sand with void. *Soils Found* 53(3):363–374
27. Huckert A et al (2016) Load transfer mechanisms in geotextile-reinforced embankments overlying voids: experimental and analytical approaches. *Geotext Geomembr* 44(3):442–456
28. Feng S-J et al (2017) An analytical method for predicting load acting on geosynthetic overlying voids. *Geotext Geomembr* 45(6):570–579
29. Lai F, Chen F, Li D (2018) Bearing capacity characteristics and failure modes of low geosynthetic-reinforced embankments overlying voids. *Int J Geomech* 18(8):04018085
30. Zhou H et al (2018) Bearing capacity of strip footings on c-φ soils with square voids. *Acta Geotech* 13:747–755
31. Wu G et al (2020) Effect of eccentric load on the undrained bearing capacity of strip footings above voids. *Int J Geomech* 20(7):04020078
32. da Silva Burke T, Elshafie M (2021) Geosynthetic-reinforced soils above voids: Observation and prediction of soil arching. *Geotext Geomembr* 49(3):579–592

33. da Silva Burke T, Elshafie M (2021) Geosynthetic-reinforced soils above voids: Observation of soil and geosynthetic deformation mechanisms. *Geotext Geomembr* 49(1):1–18
34. Anaswara S, Shivashankar R (2021) Study on behaviour of two adjacent strip footings on unreinforced/reinforced granular bed overlying clay with voids. *Geotech Geol Eng* 39(3):1831–1848
35. Chaabani W, Remadna MS, Abu-Farsakh M (2022) Numerical modeling of the ultimate bearing capacity of strip footings on reinforced sand layer overlying clay with voids. *Infrastructures* 8(1):3
36. Tizpa P, Chenari RJ, Payan M (2023) PFC/FLAC 3D coupled numerical modeling of shallow foundations seated on reinforced granular fill overlying clay with square void. *Comput Geotech* 161:105574
37. Khosravi S et al (2024) Undrained Bearing Capacity of Circular and Square footings above Centric and Eccentric three-dimensional cavities. *Int J Geomech* 24(6):04024104
38. Naftchali FM, Bathurst RJ (2024) Numerical modelling of reinforced fill over a void considering rate-dependent stiffness of the reinforcement. *Geotextiles and Geomembranes*
39. Komak Panah A, Yazdi M, Ghalandarzadeh A (2015) Shaking table tests on soil retaining walls reinforced by polymeric strips. *Geotext Geomembr* 43(2):148–161
40. Safaei AM, Mahboubi A, Noorzad A (2021) Experimental investigation on the performance of multi-tiered geogrid mechanically stabilized earth (MSE) walls with wrap-around facing subjected to earthquake loading. *Geotext Geomembr* 49(1):130–145
41. Ren F, Huang Q, Chen J (2022) Centrifuge modeling of geosynthetic-reinforced soil retaining walls subjected to the combined effect of earthquakes and rainfall. *Geotext Geomembr* 50(3):470–479
42. Panah AK, Eftekhari Z (2021) Shaking table tests on polymeric-strip reinforced-soil walls adjacent to a rock slope. *Geotext Geomembr* 49(3):737–756
43. Xu P, Hatami K, Jiang G (2020) Shaking table study of the influence of facing on reinforced soil wall connection loads. *Geosynthetics Int* 27(4):364–378
44. Xu P, Hatami K, Jiang G (2021) Shaking table performance of reinforced soil retaining walls with different facing configurations. *Geotext Geomembr* 49(3):516–527
45. Mehrjardi GT, Ghanbari A, Mehdizadeh H (2016) Experimental study on the behaviour of geogrid-reinforced slopes with respect to aggregate size. *Geotext Geomembr* 44(6):862–871
46. ASTM (2017) Standard test method for tensile properties of geotextiles by the wide-width strip method
47. ASTM D (6637) Standard test method for determining tensile properties of geogrids by the single or multi-rib tensile method. in American Society for Testing and Materials. 2015
48. Milligan G, Fannin R, Farrar D (1986) Model and full-scale tests of granular layers reinforced with a geogrid. in Proceedings of third international conference on geotextiles
49. Adams MT, Collin JG (1997) Large model spread footing load tests on geosynthetic reinforced soil foundations. *J Geotech Geoenviron Eng* 123(1):66–72
50. Astm D (2011) Standard test method for direct shear test of soils under consolidated drained conditions. D3080/D3080M, 3(9)
51. ASTM D (2012) Standard test methods for laboratory compaction characteristics of soil using standard effort (12 400 ft-lbf/ft³ (600 kN-m/m³)). D698-12
52. ASTM AD (2014) 854–14 Standard Test Methods for Specific Gravity of Soil Solids by Water Pycnometer 1, ASTM Int. West Conshohocken, Pa
53. Soil ACD-o. and Rock (2017) Standard practice for classification of soils for engineering purposes (unified soil classification system) 1. ASTM international
54. Terzaghi K (1943) Theoretical soil mechanics
55. Akinmusuru JO, Akinbolade JA (1981) Stability of loaded footings on reinforced soil. *J Geotech Eng Div* 107(6):819–827
56. Ghosh A, Ghosh A, Bera AK (2005) Bearing capacity of square footing on pond ash reinforced with jute-geotextile. *Geotext Geomembr* 23(2):144–173
57. Shukla S, Sivakugan N (2009) A general expression for geosynthetic strain due to deflection. *Geosynthetics Int* 16(5):402–407
58. Yang Z (1972) Strength and deformation characteristics of reinforced sand. University of California, Los Angeles
59. Bathurst RJ, Karpurapu R (1993) Large-Scale Triaxial Compression Testing of Geocell-Reinforced Granular Soils. *Geotechnical testing journal*, pp. 296–303

Publisher's Note Springer Nature remains neutral with regard to jurisdictional claims in published maps and institutional affiliations.

Springer Nature or its licensor (e.g. a society or other partner) holds exclusive rights to this article under a publishing agreement with the author(s) or other rightsholder(s); author self-archiving of the accepted manuscript version of this article is solely governed by the terms of such publishing agreement and applicable law.